Direct detection of exoplanets in the 3–10 μm range with E-ELT/METIS

Sascha P. Quanz[1], Ian Crossfield[2], Michael R. Meyer[1], Eva Schmalzl[3] and Jenny Held[4]

[1]*Institute for Astronomy, ETH Zurich, Wolfgang-Pauli-Strasse 27, 8093 Zurich, Switzerland*
e-mail: sascha.quanz@astro.phys.ethz.ch
[2]*Max Planck Institute for Astronomy, Konigstuhl 17, 69117 Heidelberg, Germany*
[3]*Leiden Observatory, Leiden University, P.O. Box 9513, 2300 RA Leiden, The Netherlands*
[4]*Department of Physics, ETH Zurich, 8093 Zurich, Switzerland*

Abstract: We quantify the scientific potential for exoplanet imaging with the mid-infrared E-ELT Imager and Spectrograph (METIS) foreseen as one of the instruments of the European Extremely Large Telescope (E-ELT). We focus on two main science cases: (1) the direct detection of known gas giant planets found by radial velocity (RV) searches; and (2) the direct detection of small ($1-4\,R_{\oplus}$) planets around the nearest stars. Under the assumptions made in our modelling, in particular on the achievable inner working angle and sensitivity, our analyses reveal that within a reasonable amount of observing time METIS is able to image >20 already known, RV-detected planets in at least one filter. Many more suitable planets with dynamically determined masses are expected to be found in the coming years with the continuation of RV-surveys and the results from the GAIA astrometry mission. In addition, by extrapolating the statistics for close-in planets found by Kepler, we expect METIS might detect ≈ 10 small planets with equilibrium temperatures between 200 and 500 K around the nearest stars. This means that (1) METIS will help constrain atmospheric models for gas giant planets by determining for a sizable sample their luminosity, temperature and orbital inclination; and (2) METIS might be the first instrument to image a nearby (super-) Earth-sized planet with an equilibrium temperature near that expected to enable liquid water on a planet surface.

Received 26 October 2013, accepted 2 April 2014, first published online 17 June 2014

Key words: high angular resolution, infrared, instrumentation, planetary systems.

Introduction

Since the discovery of the first exoplanet orbiting a Sun-like star in 1995 (Mayor & Queloz 1995) radial velocity (RV) measurements and transit photometry have been the dominant techniques for the detection and characterization of exoplanets. Long-term ground-based RV surveys and in particular NASA's space mission Kepler enable us to constrain the occurrence rate of planets around other stars as a function of planetary mass, size, and orbital period. Mayor *et al.* (2011) presented RV statistics for Solar-type host stars and planets with periods out to 10 years and minimum masses as low as $\sim 3-10\,M_{\oplus}$. Similarly, Howard *et al.* (2012) analysed the occurrence rate of planets with sizes >2 $R_{\oplus}$ and orbital periods $\leqslant 50$ days (~ 0.25 AU) around Solar-type stars using Kepler data. Both studies demonstrated that low-mass/small planets are much more frequent than massive/large planets.

As the probability of observing a planet transiting in front of its host stars decreases with orbital separation and as the detection of a planet by RV measurements normally requires the coverage of a full orbit, these two techniques typically reveal planets in the inner few AU around a star. This means that in order to get a census of exoplanets at larger orbital separations other techniques have to complement RV and transit searches. The two most important techniques here are microlensing (e.g. Cassan *et al.* 2012) and direct imaging. We will focus on the latter one throughout this paper.

Numerous direct imaging surveys carried out in the last years rule out the existence of a large population of massive gas giants planets ($\gtrsim 2\,M_{Jupiter}$) on wide orbits ($\gtrsim 50$ AU) (e.g. Lafrenière *et al.* 2007; Chauvin *et al.* 2010; Heinze *et al.* 2010; Rameau *et al.* 2013b; Biller *et al.* 2013; Nielsen *et al.* 2013; Janson *et al.* 2013; Wahhaj *et al.* 2013)[1]. However, a few fascinating systems were revealed by direct imaging (Marois *et al.* 2008, 2010; Kalas *et al.* 2008; Lagrange *et al.* 2010; Rameau *et al.* 2013a; Carson *et al.* 2013; Kuzuhara *et al.* 2013) partly challenging our understanding of the formation and atmospheric properties of gas giant planets. The key challenge for direct imaging is to obtain a high-contrast performance at very small inner working angles (IWA) so that the faint signal of a planetary companion can be detected and separated from the strong signal of the nearby star. If successful, the direct detection of photons from an exoplanet offers a unique pathway to study and characterize the planet's atmospheric properties. Transit or secondary eclipse photometry

---

[1] We only list surveys with $\geqslant 50$ stars.

and spectroscopy can in principle also be used to probe the atmosphere of exoplanets directly and currently these techniques produce most of the corresponding results (e.g. Seager & Deming 2010). However, typically only close-in planets can be studied in this way because the probability of transit declines with increasing semi-major axis. As the orbital inclination of exoplanets is randomly distributed in the sky when seen from the Earth, the vast majority of the overall exoplanet population does *not* transit in front of and behind their host star. In order to investigate these objects and study exoplanet atmospheres covering a wide range of planetary masses and orbital separations, direct imaging observations – ground-based or space-based – are essential.

Currently, dedicated high-contrast exoplanet imagers are being installed at 8 m telescopes: SPHERE at the Very Large Telescope (VLT) (Beuzit *et al.* 2006) and GPI on Gemini South (Macintosh *et al.* 2006). These instruments work in the optical and/or near-infrared (NIR) and, depending on their final on-sky performance, they are expected to detect gas giant planets down to 10 AU or so around young, nearby stars. Smaller and shorter period planets are typically beyond the reach of these instruments as their contrast performance, sensitivity and spatial resolution are still insufficient[2].

In this paper, we quantify two exoplanet imaging science cases for ground-based Extremely Large Telescopes (ELTs). Our focus is on the 3–10 μm wavelength range, which is normally dominated by thermal emission from the planets rather than by reflected starlight. We take METIS (Brandl *et al.* 2012) as our default instrument in our analyses. METIS could be the third instrument installed at the 39 m European Extremely Large Telescope (E-ELT) according to the E-ELT instrumentation roadmap[3]. It is AO-assisted and currently foreseen to offer imaging and medium-resolution spectroscopy over the full L, M and N band wavelength range (3–14 μm). High-resolution integral field spectroscopy is planned for the L and M bands (3–5.3 μm). In the following sections we motivate the use of this wavelength range for exoplanet research and quantify two major exoplanet science cases for METIS: (a) the fraction of the currently known exoplanets detected by RV that can be imaged with E-ELT/METIS; and (b) the prospects of directly detecting small planets around nearby stars. Finally, we discuss our findings and conclude in the final section.

Motivation for thermal IR imaging of exoplanets from the ground

The motivation to exploit thermal IR wavelengths[4] for exoplanet imaging has a scientific and a technical aspect.

Scientific considerations

By observing at thermal IR wavelengths a slightly different part of the exoplanet parameter space is probed compared to observations in the NIR. This becomes clear just by considering Wien's law and estimating the blackbody temperatures that correspond to the central wavelength of each filter. For the direct detection of thermal emission from self-luminous gas giant exoplanets, for a given age, one is able to probe less massive planets or, for a given mass, one is able to search around older stars. This is a direct consequence of the very red IR colours of planetary mass objects and the fact that they contract and cool during their evolution (for theoretical work on gas giant planet evolution and luminosities see, e.g. Chabrier *et al.* 2000; Burrows *et al.* 2001; Baraffe *et al.* 2003; Sudarsky *et al.* 2003; Marley *et al.* 2007; Fortney *et al.* 2008; Spiegel & Burrows 2012). A nice example, demonstrating the power of observing in the thermal IR, is provided by the recently discovered planetary mass companion to the A-type star HD95086 by Rameau *et al.* (2013a). While the planet was clearly detected in the L band (3.8 μm) it remained undetected in H and Ks (∼ 1.6 and 2.3 μm; Meshkat *et al.* 2013; Rameau *et al.* 2013a).

Another aspect is the search for planets that are still somewhat embedded in the circumstellar discs of their host stars. The opacities of dust grains typically found in these discs have wavelength dependent extinction effects, with shorter wavelength photons being more strongly affected. Hence, it could be possible to detect young planets in the thermal IR that remain unseen at NIR wavelengths. A possible example is the candidate protoplanet detected in the disc around the young intermediate mass star HD100546. Quanz *et al.* (2013) detected the object in the L band. If all of the observed flux arose from the photosphere of a 'normal' low-mass companion its mass would be 15–20 $M_{Jupiter}$ according to theoretical models. Boccaletti *et al.* (2013) analysed K band data from Gemini/NICI of the same star and were not able to detect the companion candidate even though the data were good enough to see a 15–20 $M_{Jupiter}$ object based on the same models. Whether extinction is the dominant effect here or whether the intrinsic properties of the object only allow for detection in the L band is still to be investigated, but it clearly shows that observations at thermal IR wavelengths can reveal objects that are not easily accessible with NIR observations.

For old exoplanets, depending on the instrument performance and the properties of the exoplanetary system, it might be 'easier' to detect reflected starlight from the planet at optical or NIR wavelengths than thermal emission at longer wavelengths. However, typically thermal emission from planets depends significantly less on the orbital phase and orbital inclination of the object compared to observations in reflected light. Also, reflected light observations give only access to the product of atmospheric albedo and planet radius and additional observations are required to break the degeneracy. Having an estimate for the effective temperature of the planet from its thermal emission and knowing the distance to the object directly yields its radius. We emphasize

---

[2] The ZIMPOL sub-instrument of SPHERE should be able to detect polarized, reflected light of close-in gas giant planets at optical wavelengths around the nearest stars (Schmid *et al.* 2006).
[3] see, http://www.eso.org/sci/facilities/eelt/instrumentation/
[4] Throughout this paper we use the term thermal IR for the 3–10 μm wavelength range while NIR refers to 1–2.5 μm.

that in the ideal case one wants to combine the information obtained from thermal emission *with* those from reflected light. This provides complementary insights into atmospheric properties and allows for a significantly higher degree of characterization (see, e.g. Seager 2013).

Finally, once a planet has been detected, it is important to understand the diagnostic power of different wavelength bands for the characterization of the object. Concerning potential atmospheric constituents it is worth recalling that the L, M and N bands include some main molecular features, for example CH_4 (3.3 μm), CO (4.7 μm) and O_3 (4.7, 9.6 μm). In particular for the gas giant planets that have already been directly imaged (e.g. the HR8799 system) the spectral energy distribution (SED) in the L band between 3.2 and 4.0 μm is of substantial diagnostic power to constrain the ratio between CO and CH_4 in the atmosphere and to search for potential chemical disequilibrium (e.g. Hinz *et al.* 2010; Skemer *et al.* 2012). Additional indications for chemical disequilibrium could also come from the very red end of the L band. Janson *et al.* (2011) took a low-resolution L band spectrum of the exoplanet HR8799 c and found an apparent deficiency in flux beyond 4 μm as predicted by non-equilibrium atmospheric models. In addition, clouds seem to play a crucial role in shaping the SEDs of these massive planets. Also here, the L band regime proves to be an important diagnostic window (e.g. Lee *et al.* 2013). Turning to smaller, rocky planets it turns out that the N band could potentially be used to constrain the surface composition of warm/hot objects. Hu *et al.* (2012) presented simulations of 8–13 μm spectra for rocky planets with different surface temperatures and compositions. Surface characterization could provide a powerful method to unambiguously identify a rocky, airless exoplanet.

Technical considerations

As mentioned above, the direct detection and characterization of exoplanets requires high-contrast performance at very small IWA. Given their very different effective temperatures, the flux contrast between stars and planets in the 3–10 μm range is less stark than at optical or NIR wavelengths. Hence, the instrument requirements in terms of achievable contrast performance can be less stringent for observations in the thermal IR. In addition, AO systems on large ground-based telescopes provide higher Strehl ratios at thermal IR wavelengths compared to the optical or NIR. This, again, helps to tackle the contrast problem as more light from the central star is concentrated in the core of the point spread function (PSF) and less flux is left in the uncorrected halo. AO-assisted thermal IR imagers provide Strehl ratios in the L and M bands that are at least comparable, if not superior, to the expected Strehl ratios of the next generation high-contrast imagers working in the NIR. LMIRCam at the Large Binocular Telescope (LBT) is equipped with an adaptive secondary mirror and typically reaches Strehl ratios of 80–90% in the L and M bands. This is also the goal for the planned ERIS instrument at the VLT.

The key challenge to overcome, when observing in the thermal IR from the ground, is the background emission from the sky, the telescope and the optical components within the instrument. On the one hand, the photon noise from these contributions sets the ultimate detection limit for a given observing time, but temporal fluctuations in the background pose an additional problem. Great improvements can be made if this issue is taken into account already in the design phase of an instrument by minimizing the amount of 'warm' components in the light path. Good examples are CLIO, formerly installed at the Multiple Mirror Telescope (MMT), LBT/LMIRCam and VLT/ERIS.

A technical goal for high-contrast imaging at thermal IR wavelengths is to move the background-limited regime as close as possible to the central star. If one is background-limited and not contrast-limited then – to first order – by increasing the observing time, higher sensitivities can be reached (the signal-to-noise ratio (SNR) is then proportional to $\sqrt{t}$ with t being the integration time). Different coronagraphic designs to cancel out the diffraction rings around the central star have been developed in recent years specifically for observations between 3 and 10 μm. Some of them have been installed on 8 m telescopes (e.g. NACO/APP, NACO/AGPM; Kenworthy *et al.* 2010; Mawet *et al.* 2013). Typically, these coronagraphs in combination with optimized imaging techniques (e.g. Angular Differential Imaging (ADI); Marois *et al.* 2006) and advanced data reduction algorithms (e.g. PynPoint; Amara & Quanz 2012) aim at moving the background limit (BGL) as close as $2\lambda_{cen}/D$ to the star, which would then correspond to the high-contrast IWA of the imaging system.

One key aspect we would like to emphasize is that with the advent of 25–40 m diffraction-limited telescopes, observations at thermal IR wavelengths become significantly more efficient. In the sky background-limited case and for a given SNR the time to complete an observation scales as $t \propto D^{-4}$, which is an enormous advantage for future extremely large telescopes compared to current 8 m class telescopes.

Exoplanet imaging science with E-ELT/METIS

Two major exoplanet imaging science cases for E-ELT/METIS will be: (a) imaging known exoplanets detected by RV; and (b) directly detecting small planets around nearby stars. Both science cases will be quantified in the following subsections, but we emphasize that in addition to these there are other exoplanet science cases that E-ELT/METIS will be able to tackle. These include, for instance, a classical survey for gas giant and icy planets around the nearest stars; a search for young, forming planets still embedded in the circumstellar disc of their host stars; constraining atmospheric composition of cool gas giant planets (e.g. Janson *et al.* 2011); or measuring molecular abundances and wind speeds in the atmospheres of hot giant planets using high-resolution spectroscopy (e.g. Snellen *et al.* 2010; Brogi *et al.* 2012; Birkby *et al.* 2013).

As mentioned above, for the following analyses we focus on the imaging performance of METIS and do not consider spectroscopic applications. METIS will offer diffraction-limited imaging in the L, M and N bands with a field-of-view

Table 1. *E-ELT/METIS filter and performance estimates*

Filter	λ_{cen} (µm)	Filter width (µm)	IWA[a] (″)	Sensitivity[b] (µJy)	Limiting magnitude[b,c]
L	3.58	0.98	0.038	0.27	22.4
M	4.78	0.60	0.051	2.76	19.3
N	10.6	5.2	0.112	9.84	–

[a] We assume to be background limited down to an IWA of $2\lambda_{cen}/D$.

[b] 5σ detection limits in 3 h of telescope time incl. 20% overhead, i.e. 8640 s effective on source integration time. These values assume a cold-stop in the instrument design that leads to an effective telescope diameter of $D = 37$ m and has an inner obscuration of 11.1 m.

[c] As the exact filter profiles are not defined yet, the zero points were estimated based on www.not.iac.es/instruments/notcam/ReferenceInfo/conver.html and should be good to 5–10%. As none of our analyses requires a limiting magnitude in the N band, we do not provide an estimate here.

(FoV) of approximately $18'' \times 18''$[5]. The assumed sensitivity limits for each band correspond to a 3 h observing block.

For deep planet searches using the ADI technique such an observing block is typically centred on the targets' meridian passage to maximize the amount of field rotation. As METIS will be situated on Cerro Armazones in Chile, for our final analyses we only consider objects with a declination <30°, which ensures the airmass is <2.0 for all objects. In Table 1, we summarize the assumed filter properties, the IWA and the sensitivity estimates for the different bands.

Direct detection of planets found by RV surveys

Direct imaging of planets found by RV surveys offers major opportunities. Irrespective of the age of the system, multiple epoch observations yield the orbital inclination of the planet and allow for the derivation of the planet's true mass. This information, together with the observed brightness (possibly in multiple bands) and host star properties, can then be used to characterize individual planets and to constrain atmospheric models of planetary mass objects. At young ages, direct imaging is the only technique that can break some of the degeneracies existing in the atmospheric and evolutionary models of gas giant planets and to constrain the initial conditions for gas giant planet formation. As these conditions are basically unknown, a huge spread in fundamental planet parameters (e.g. radius and temperature) is found for ages $\lesssim 200$ Myr, depending on what initial conditions are chosen (e.g. Spiegel & Burrows 2012). Up to now, β Pic b is the only young planet, where we have images as well as at least some mass constraints derived from RV measurements (Lagrange *et al.* 2012).

In the following, based on the current census of exoplanets discovered by RV, we quantify how many planets an instrument such as METIS at the E-ELT could detect. To do so, we retrieved the list of known exoplanets detected by RV from the exoplanet.eu database (as of July 29, 2013; Schneider *et al.* 2011). Not all relevant parameters are known for all of these systems. To be conservative we disregarded objects with unknown values for the semi-major axis a, orbital period P, distance from the Earth to the host star d or argument of

periastron ω. In cases where the orbital eccentricity e was not known, we conservatively assumed $e = 0$. If the orbits were, however, eccentric, the planets would be easier to detect as they would spend more time at larger separations from their host star. For systems with no estimate for the age, we assumed an age of 5 Gyr, which is the average age of the planets with age estimates.

Furthermore, we only considered objects with a minimum mass of $m \cdot \sin(i) > 0.3 \, M_{Jupiter}$. Initial estimates suggested that planets with lower minimum masses would not be easily detectable with our underlying assumptions. This is supported by our final results, where the lowest mass planet that is detectable has $m \cdot \sin(i) > 1 \, M_{Jupiter}$ (see below) even though numerous planets with masses $0.3 \, M_{Jupiter} < m \cdot \sin(i) < 1.0 \, M_{Jupiter}$ were included in the input sample. In total, the initial input sample had 352 objects, still including objects from both the Northern and Southern hemisphere.

We used the COND atmospheric models (Baraffe *et al.* 2003) to compute the apparent L and M band magnitudes for the planets as a function of age and minimum mass. This approach is again conservative in two ways: (1) using the given minimum mass to estimate the planets' brightness is conservative, as planets with higher masses would be brighter and hence easier to detect at all ages; (2) for some planets the expected equilibrium temperature T_{eq} may exceed the effective temperature predicted by the COND models $T_{eff,model}$ in which case the planets' brightness is also underestimated.

In a next step, we estimated the typical on-sky separation between the planet and its host star and compared it to the assumed IWA of METIS in the L and M bands. In cases where the orbital inclination i of the planet is known (or at least estimated), it is straight forward to compute the apparent separation between planet and star as a function of time. For most RV planets, however, i and also the longitude of the ascending node Ω are unknown. We did a Monte Carlo simulation for these two variables to estimate the probability distribution of the on-sky separation knowing all the other orbital parameter. We then only kept (1) planets with known i where the apastron passage exceeds a separation of $2\lambda_{cen}/D$, and (2) planets with unknown i and Ω, where the probability of finding the planet at a separation $> 2\lambda_{cen}/D$ exceeds 50%, if one were to observe the object at a random time. This selection resulted in 130 and 95 objects in the L and M bands, respectively. We then excluded 25 objects in the L band and 19

[5] The FoV is large enough as not to put any constraints on the planet detections discussed in this paper. The on-sky separation between the planets considered here and their host stars is significantly smaller.
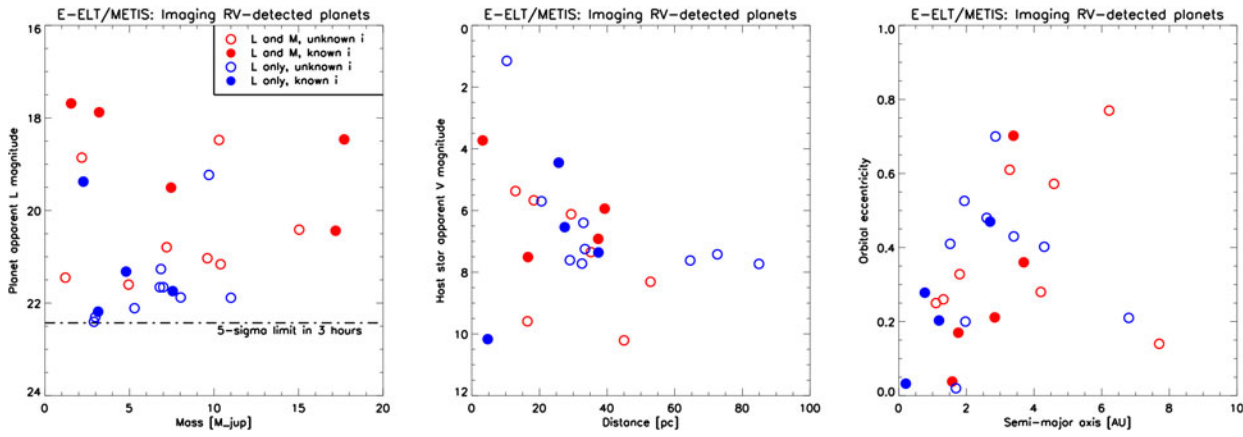
Fig. 1. Properties of RV-detected planets that can be directly imaged with E-ELT/METIS. Symbols are the same in all panels. Left panel: Apparent L magnitude of planets detected by RV as a function of their minimum mass. The dash-dotted line indicates the 5 σ detection limit (see, Table 1). Blue dots show planets that are only detectable in the L band (13 objects) and red dots planets that are detectable in the *L* and *M* band (13 objects). Filled dots are objects with an estimate for their orbital inclination *i*, open dots are objects with unknown *i*. Middle panel: Host star apparent V band magnitude as a function of distance for detectable planets. Right panel: Orbital eccentricity as a function of semi-major axis for detectable planets.

objects in the M band because their declination was higher than our assumed limit.

Finally, we compared the estimated L and M band magnitudes of the remaining objects to our assumed 5 σ sensitivity limits (Table 1). Figure 1 shows that, given the selection criteria described above, METIS is capable of directly detecting 26 of the known gas giant planets in the L band, 13 of which are also detectable in the M band. The planets cover a range in minimum mass roughly between 1 and 18 M_{Jupiter} and their host stars span a wide magnitude range for a given distance, which indicates an interesting spread in both planet and also host star properties. Furthermore, the planets span a wide range in semi-major axis and also orbital eccentricity. This leads to a wide range of planetary temperatures across the whole sample, but also to significant changes in stellar insolation for individual planets on highly eccentric orbits. A first-order estimate for the expected equilibrium temperature reveals that two planets (HD 62509 b and HD 60532 b) likely have effective temperatures higher than those predicted by the models applied in our selection process. Hence, these planets should appear even brighter and be easier to detect than shown here. Finally, three of the planets reside in stellar binary systems (HD196885 A b, HD106515 A b and GJ676 A b), and there are two systems where two planets can be detected (HD 60532 b,c and HD 128311 b,c). These latter systems potentially allow a direct comparison of gas giant properties within extrasolar planetary systems. Other stars have additional planets as well, but those are below the detection limits chosen here. We list all planets and their key properties in Table 2.

Detecting small planets

One of the mid- to long-term goals of exoplanet research is certainly the direct detection and characterization of rocky – and potentially habitable – planets. It is useful to consider what ELTs might be able to deliver in this context (cf. Hinz *et al.*

2009). In a first step, we provide some first-order estimates of what parameter space in terms of planet size, temperature and host star properties E-ELT/METIS will be able to probe, depending on the observing wavelength. In a second step, we carry out an updated version of the Monte Carlo experiment first presented by Crossfield (2013) to quantify, how many planets we can expect to detect based on the occurrence rate of planets found by the Kepler mission.

Small planet parameter space probed by E-ELT/METIS

The following first-order estimates provide some interesting insights about the prospects of imaging small planets with E-ELT/METIS. We consider three planetary sizes (1, 2 and 3 $R_{\oplus}$) and five different effective temperatures for these planets approximated as blackbody emission (255, 300, 400, 500, 600 K). Varying the distance between the Earth and these planets, we compute the flux density received at the Earth in different wavebands. As a benchmark test it is useful to recall that the Earth seen from 10 pc distance emits approximately 0.4 μJy at 10.5 μm assuming blackbody emission coming from its surface (Des Marais *et al.* 2002).

In order to assess if certain types of planets can be directly imaged with METIS, we further need to take into account the sensitivity limits in each filter and also the IWA achievable at each observing wavelengths (Table 1). As described above, we assume that the BGL can be achieved at $2\lambda_{\mathrm{cen}}/D$ and we take this separation as IWA. Finally, we assume that the planet's effective temperature corresponds to its equilibrium temperature T_{eq}, which depends on the luminosity of the star, the planet's Bond albedo A_B, and the separation from the host star r_p:

$$T_{\mathrm{eq}} = \left[\frac{L_*(1 - A_B)}{4\pi\sigma}\right]^{1/4} \left(\frac{1}{2r_p}\right)^{1/2}.$$

Table 2. *Key properties of planets detected by RV surveys that can be imaged with E-ELT/METIS (see text for selection criteria). All values were adopted from the exoplanet.eu database (unless indicated otherwise) except for the apparent L magnitude and the M band flag, which were derived here (see the subsection 'Direct detection of planets found by RV surveys')*

Name	Minimum mass ($M_{Jupiter}$)	Apparent L (mag)	Distance (pc)	Age (Gyr)	a (AU)	e	Known i	M band[a]
HD 82943[b]	4.8	21.3	27.5	3.1	1.2	0.20	yes	no
HD 60532[b]	3.2	22.2[b]	25.7	2.7	0.8	0.28	yes	no
HD 60532[c]	7.5	19.5	25.7	2.7	1.6	0.04	yes	yes
eps Eridani[b]	1.6	17.7	3.2	0.7	3.4	0.70	yes	yes
HD 168443[c]	17.2	20.4	37.4	9.8	2.8	0.21	yes	yes
HD 38529[c]	17.7	18.5	39.3	3.3	3.7	0.36	yes	yes
HD 128311[c]	3.2	17.9	16.6	0.4	1.8	0.17	yes	yes
Gliese 876[b]	2.3	19.4	4.7	2.5	0.2	0.03	yes	no
HD 106252[b]	7.6	21.7	37.4	5.0	2.7	0.47	yes	no
HD 128311[b]	2.2	18.9	16.6	0.4	1.1	0.25	no	yes
HD 147513[b]	1.2	21.5	12.9	0.7	1.3	0.26	no	yes
HD 196885 A[b]	3.0	22.3	33.0	2.0	2.6	0.48	no	no
HD 125612[d]	7.2	20.8	52.8	2.1	4.2	0.28	no	yes
HD 86264[b]	7.0	21.7	72.6	2.2	2.9	0.70	no	no
HD 141937[b]	9.7	19.2	33.5	2.6	1.5	0.41	no	no
HD 74156[c]	8.0	21.9	64.6	3.7	3.4	0.43	no	no
HD 39091[b]	10.3	18.5	18.3	3.8	3.3	0.61	no	yes
HD 81040[b]	6.9	21.3	32.6	4.2	1.9	0.53	no	no
HD 106270[b]	11.0	21.9	84.9	4.3	4.3	0.40	no	no
HD 111232[b]	6.8	21.7	29.0	5.2	2.0	0.20	no	no
HD 142[c]	5.3	22.1	20.6	5.9	6.8	0.21	no	no
HD 106515 A[b]	9.6	21.0	35.2	6.0	4.6	0.57	no	yes
HIP 5158[c]	15.0	20.4	45.0	6.0	7.7	0.14	no	yes
HD 219077[b]	10.4	21.2	29.4	8.9	6.2	0.77	no	yes
HD 62509[b]	2.9	22.4[b]	10.3	5.0[c]	1.7	0.02	no	no
GJ 676 A[b]	4.9	21.6	16.5	5.0[c]	1.8	0.33	no	yes

[a] Flag indicating whether object is also detected in the M band within the given detection limits.
[b] L band brightness likely underestimated as first-order estimates suggest $T_{eff,model} < T_{eq}$ (see text).
[c] Age assumed for analysis as no age was given in exoplanet.eu database (see text).

Using the Earth as reference case with $T_{eq} = 255$ K, $r_p = 1$ AU, $L_* = 1\,L_\odot$ and $M_* = 1\,M_\odot$, and recalling $T_{eq} \propto 1/\sqrt{r_p}$, we can estimate the planet–star separation that corresponds to different T_{eq}. For example, around the Sun, $T_{eq} = 500$ K corresponds to a separation of 0.26 AU. In order to be able to consider different spectral types for the host star, we approximate $T_{eq} \propto L_*^{1/4}$ and $L_* \propto M_*^4$, which leads to $T_{eq} \propto M_*$. Hence, for an F star with a mass of 1.5 $M_\odot$ we find $T_{eq} = 383$ K at 1 AU and, correspondingly, $T_{eq} = 255$ K at 2.25 AU. Knowing the IWA of our instrument for a given wavelength we can now directly compare its value with the projected separation of any given planet–host star combination. We considered five host star types defined by their mass (0.5 $M_\odot$ (M-type), 0.75 $M_\odot$ (K-type), 1.0 $M_\odot$ (G-type), 1.5 $M_\odot$ (F-type) and 2.0 $M_\odot$ (A-type)).

Figure 2 shows the results. The basic trends are intuitively clear: The hotter, the bigger and the more nearby the planet, the more flux is received at the Earth. As hotter planets have to be closer to their host star, depending on the host star's spectral type, we reach the IWA of the telescope where we can no longer spatially separate the planet from the star at a certain distance from the Earth. While hotter planets emit more flux, the space volume we can probe, where we still spatially resolve them from their stars, is much smaller than for cooler planets.

Looking at some planet–star combinations more specifically, we see two key results: (1) the coolest planets in our analyses ($T_{eq} = 255$–300 K) would only be detectable in the N band around the very nearest stars and neither in the L nor the M band. (2) For all hotter planets ($T_{eq} = 400$–600 K) the L band is the best wavelength range for planet detections as for any planet–star combination the space volume probed is larger than in the other bands.

Monte Carlo simulation of small planet detections with E-ELT/METIS

To complement the analysis described above, we determined the population of planets that would be accessible to METIS observations using empirically constrained estimates of short-period planet frequency as a function of stellar type, planet radius and orbital period. To do this we used the Monte Carlo approach outlined in detail in Crossfield (2013). Briefly described, this analysis simulates thousands of plausible extrasolar planetary systems using measurements of planet frequency from the Kepler satellite (Howard *et al.* 2012) and estimates the likelihood of finding a detectable planet by comparing the planets' predicted blackbody fluxes to analytic estimates of high-contrast performance (Guyon 2005) and detection limits. Unlike in the subsection 'Direct detection of planets found by RV surveys', here the planet's thermal
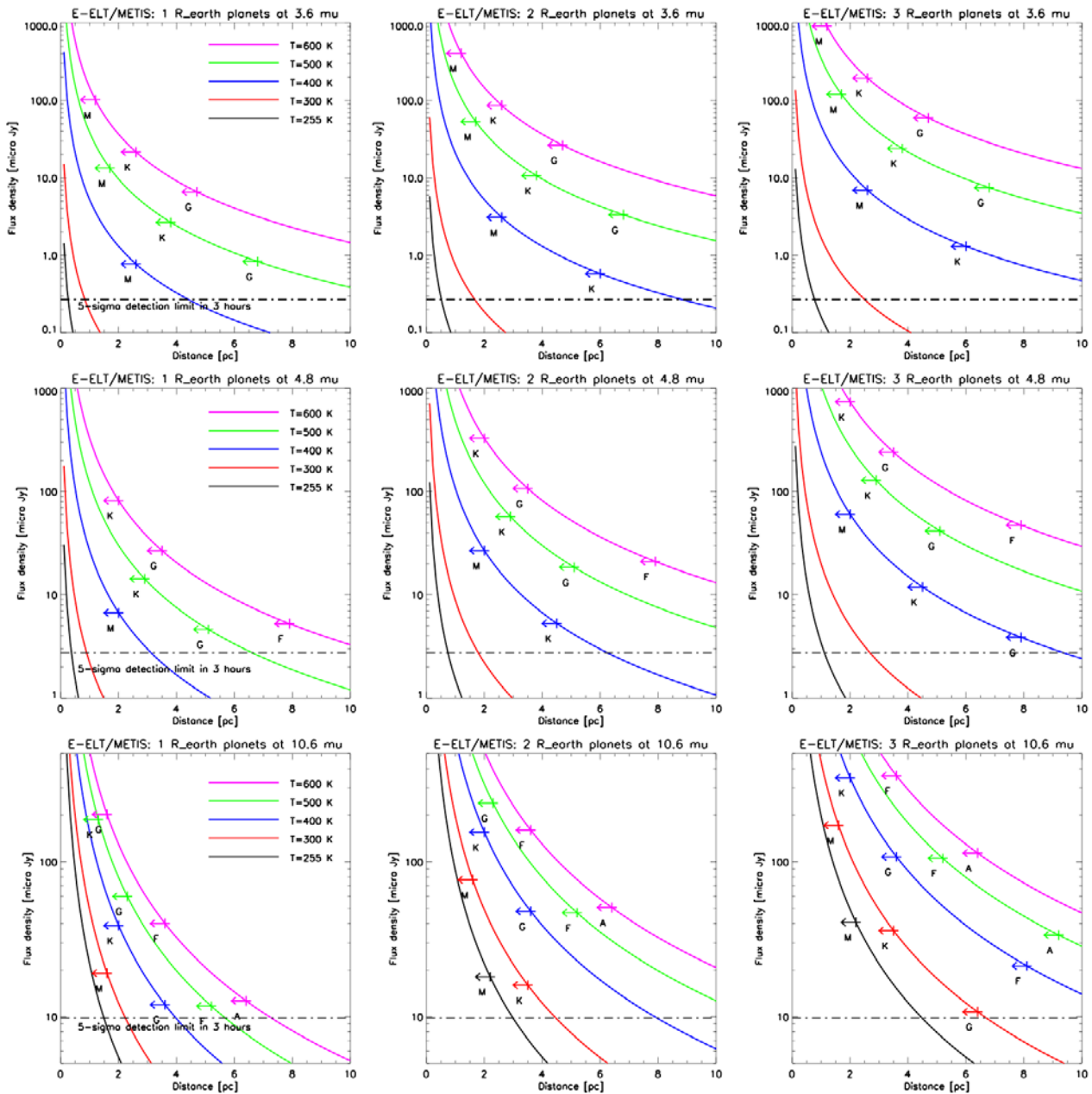
Fig. 2. First-order estimate of the parameter space of small planets that METIS can probe at different wavelengths. All plots show the flux density of different kinds of small planets as a function of their distance from the Sun and are organized as follows: Analyses for the L band (top row), M band (middle row) and N band (bottom row); planets with $1\,R_\oplus$ (left column), $2\,R_\oplus$ (middle column), and $3\,R_\oplus$ (right column). The different colours correspond to different blackbody temperatures of the planets (see legends in the left column). The arrows and the letters below them indicate out to what distance a planet with a given size and temperature can be detected around a star with a certain mass, i.e. spectral type (see text). At distances greater than this limit the assumed IWA is insufficient to spatially resolve the star–planet system in the given sensitivity limits. The dash-dotted lines denote the $5\,\sigma$ detection limit in 3 h of telescope time for each filter (see Table 1).

emission does not come from residual heat of formation, but from absorbed and reprocessed starlight. Contributions from reflected starlight to the observed planet fluxes are also taken into account. For this, the planet's bond albedo and geometric albedo are assumed to be wavelength independent and are randomly drawn from a uniform distribution between 0.0 and 0.4 (Crossfield 2013).

Compared to the original study done by Crossfield (2013), which had the goal of comparing the expected detection yield

of different wavelength regimes, instrument performances and telescope sizes, the present study is different in a number of aspects. Crossfield (2013) focused primarily on contrast performance and did not explicitly include constraints coming from sensitivity estimates. Ground-based thermal IR imaging has, however, quite severe sensitivity constraints coming from the high background emission at these wavelengths. The present analysis takes sensitivity limits explicitly into account (Table 1). Also, while Crossfield (2013) was a comprehensive
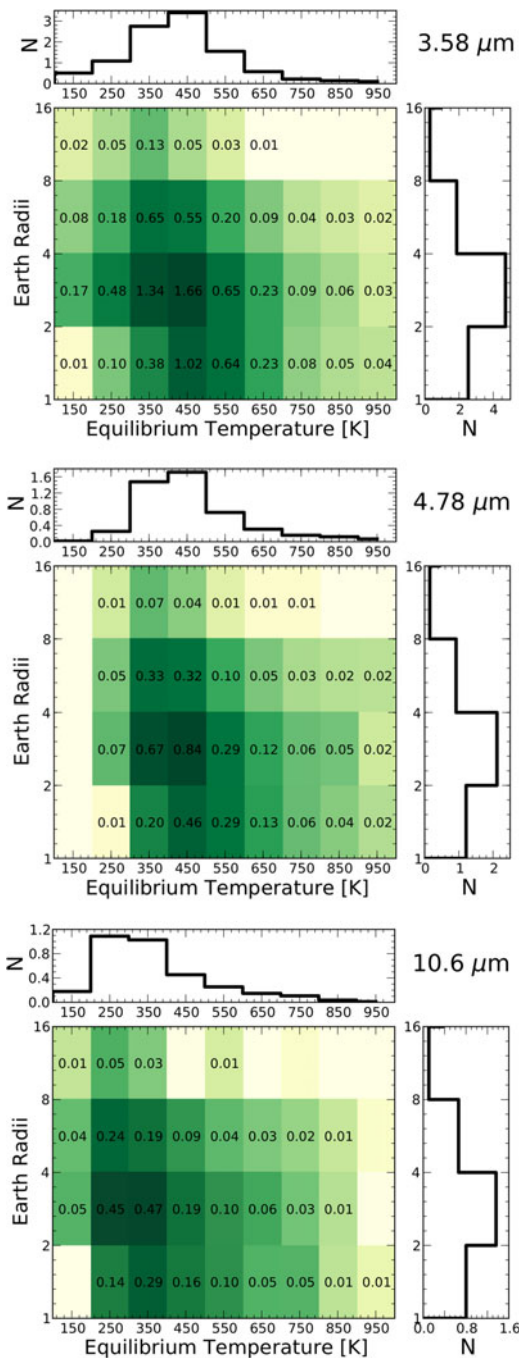
Fig. 3. 2D probability distributions for the detection of small planets using E-ELT/METIS. From top to bottom the panels show the distributions for detections in the L, M and N bands, respectively.

but partly generic case study, the present analysis is for a specific telescope and a specific instrument. The corresponding sensitivity estimates were derived using an instrument simulator (including, e.g. a model PSF, sky background noise, throughput, relevant telescope parameters). Furthermore, in light of the results presented in the previous section, we extended our analysis beyond 8 pc (as in Crossfield 2013) to include all dwarf stars with $K < 7$ mag and $d < 20$ pc. We removed close binaries, gathered stellar photometry and

parallaxes from the literature (Perryman *et al.* 1997; Monet *et al.* 2003; Cutri *et al.* 2003; Zacharias *et al.* 2012, and SIMBAD), adopted stellar radii and effective temperatures based on interferometric measurements of similar stars (Boyajian *et al.* 2012a, b, 2013), and assigned stellar masses using the V-band relation of Henry & McCarthy (1993). Selecting only objects with declination <30°, this final target list includes 246 objects; 24 of these host already known planets or planet candidates, most of which do not pass the detection threshold that we impose in our analysis, as they are either too close to the star and/or too faint. Finally, the present analysis determines how many planets are detectable in more than one filter (see below) and provides a concrete list of stars for which we summarize the detection probabilities per filter.

This new Monte Carlo analysis reveals that ≈ 10 small planets within 15 pc should be detected in at least one of the L, M or N bands. Roughly five objects could be observed in both L and M bands, and a small number (~ 2) might be observable in a combination of N and L and/or M. The results are summarized in Fig. 3, where we show the 2D probability distributions (planetary radius versus equilibrium temperature) separately for the L, M and N bands. Roughly 25% of the planets have radii of 1–2 $R_\oplus$. The rest has radii >2 $R_\oplus$ and is increasingly likely to host a substantial gaseous envelope (cf. Marcy *et al.* 2014). The expected T_{eq} of the smaller planets is ~ 100 K higher than for the larger planets. This is a selection effect: in our simulations, larger planets ($\gtrsim 4 R_\oplus$) are seen mainly in reflected starlight (even in M band); smaller planets, however, must emit relatively more thermal radiation to climb above the sensitivity threshold, and so thermal radiation comprises up to $\sim 50\%$ of their observed flux. For the L and M bands the most likely range of equilibrium temperature is 300–500 K, whereas, statistically, in the N band a couple of planets in the 200–400 K range should be found.

For the results shown in Table 3 we changed the perspective and analysed which stars in our sample are the best targets for planet searches. We only list objects where the probability of detecting a planet – regardless of size or temperature – is at least 10% in one of the observational bands. Table 3 emphasizes that, according to our simulations, the L band is the best wavelength range to search for planets, but it also shows that – based on the Kepler planet occurrence statistics – for some stars there is a fair chance to detect planets in more than one band.

Discussion

The analyses presented in the previous sections rely on some assumptions and led to some results that warrant further discussion.

Concerning the assumed sensitivity limits it is obvious that these are preliminary and are probably subject to change in the course of the METIS project. However, the values represent the current state of knowledge. Similarly, the exact filter profiles are not yet defined for METIS. This leads to some uncertainties when we compare the predicted fluxes for the RV-detected gas giant planets to the METIS detection limits

Table 3. *Summary of Monte Carlo results for specific nearby stars. All stars shown have a probability for planet detection with E-ELT/METIS of at least 10% in one of the bands. The last three columns show the detection probability in the L, M and N bands, respectively*

Name	Catalogue name	Spec. Type	Dist. (pc)	p_L	p_M	p_N
alpha Cen B[a]	HD 128621	K1V	1.3	0.59	0.65	0.74
alpha Cen A	HD 128620	G2V	1.3	0.51	0.63	0.67
Epsilon Eri[a]	HD 22049	K2V	3.2	0.47	0.32	0.32
Epsilon Ind A	HD 209100	K4V	3.6	0.46	0.26	0.14
tau Cet[a]	HD 10700	G8.5V	3.7	0.34	0.29	0.18
Proxima Cen	HIP 70890	M5.5V	1.3	0.33	–	–
Gl 166 A	HD 26965 A	K0.5V	5.0	0.32	0.17	–
delta Pav	HD 190248	G8IV	6.1	0.32	0.24	0.12
Procyon A	HD 61421	F5IV-V	3.5	0.31	0.31	0.28
Gl 887	HD 217987	M0.5V	3.3	0.28	–	–
GJ 139[a]	HD 20794	G8V	6.0	0.27	0.15	–
Gl 825	HD 202560	K7V	3.9	0.26	–	–
beta Hyi	HD 2151	G0V	7.5	0.22	0.12	–
LTT 2364	HD 38393	F6V	9.0	0.22	0.13	–
Barnard's Star	HIP 87937	M4V	1.8	0.21	–	–
zet Tuc	HD 1581	F9.5V	8.6	0.17	–	–
Gl 570 A	HD 131977	K4V	5.8	0.16	–	–
HR 4523[a]	HD 102365	G2V	9.2	0.16	–	–
gam Pav	HD 203608	F9V	9.2	0.16	–	–
LHS 348	HD 114710	G0V	9.2	0.16	–	–
LHS 2465	HD 102870	F9V	10.9	0.15	–	–
chi01 Ori	HD 39587	G0V	8.7	0.15	–	–
iot Peg	HD 210027	F5V	11.8	0.14	–	–
36 Oph C	HD 156026	K5V	5.9	0.13	–	–
gam Ser	HD 142860	F6IV	11.1	0.13	–	–
107 Psc	HD 10476	K0V	7.5	0.12	–	–
Ross 154	HIP 92403	M3.5V	3.0	0.11	–	–
Sirius A	HD 48915	A0.5V	2.6	0.11	0.11	0.10
1 Eri	HD 17206	F7V	14.0	0.11	–	–
61 Vir[a]	HD 115617	G7V	8.5	0.10	–	–

[a] Stars with known or suggested exoplanets: alpha Cen B (Dumusque *et al.* 2012), epsilon Eri (Hatzes *et al.* 2000), tau Cet (Tuomi *et al.* 2013), GJ 139 (Pepe *et al.* 2011), HR 4523 (Tinney *et al.* 2011), 61 Vir (Vogt *et al.* 2010).

because the model predictions were computed for a different filter set. However, this effect is expected to be rather small, especially compared to the uncertainties in the models themselves. Assuming that METIS will achieve background-limited performance down to an IWA as small as $2\lambda_{cen}/D$, is certainly a challenging goal, both from a technical and a data processing point of view. Until now, in some cases, the BGL was only reached at $\sim 5\lambda_{cen}/D$ (e.g. Kenworthy *et al.* 2010). The coming years will show whether the continuous progress in coronagraphic and data-processing techniques is sufficient to enable such a demanding, but scientifically crucial, performance at the E-ELT. Finally, our analyses did not take into account that, depending on the final instrument design and coronagraphs used, additional observing time is required to achieve the detection limits assumed here in a full 360° circle around the target stars. Pupil plane coronagraphs will alter the general throughout of the instrument and do not necessarily create a centrosymmetric high-contrast region around the star for separations $>2\lambda_{cen}/D$ (Kenworthy *et al.* 2010; Carlotti 2013). For focal plane coronagraphs additional overhead might be created by regular switching between the target star and a reference sky location for sky subtraction.

For the RV-detected planets it is clear that some of the orbit parameters listed in the exoplanet.eu database may be refined by future observations or that for some systems different groups obtained slightly different results. However, the selection and detection criteria we applied were rather conservative (e.g. minimum mass, $T_{eq} < T_{eff,model}$) so that detection biases introduced by uncertain orbit parameter should not have a significant effect. Also, we did not take into account any possible contribution from reflected starlight to the emission coming from the planets. This contribution is, however, indeed in most cases negligible as the planet-star flux ratio is on average $\sim 10^{-6}$ only considering the planets' thermal emission, while the flux ratio in reflected light is typically at least two orders of magnitude smaller. More importantly we need to emphasize that the possible METIS target sample might significantly change in the coming years. With increasing time baselines of RV planet surveys, additional long-period gas giant planets can expected to be found in the future, some of which yielding better detection probabilities than the objects listed here. In addition, the GAIA spacecraft will reveal additional long-period gas giant planets using high-precision astrometric measurements.

Also here we can expect additional high-priority targets for direct imaging follow-up studies with E-ELT/METIS.

The assumptions for the Monte Carlo simulations of nearby small planets and their impact on the results have been discussed in length in Crossfield (2013). One of the key assumptions is that the Kepler results for the innermost ~ 0.25 AU follow a flat distribution for wider orbits in logarithmic period space. However, this assumption is consistent with the recent analysis of four full years of Kepler data (Petigura *et al.* 2013). Once a planet candidate has been imaged around a nearby star, follow-up observations within a few months will not only be able to confirm common proper motion of the planet and its host star, but they allow also for a robust determination of the planet's orbit and hence of the received stellar insolation as a function of orbital phase. An assessment of whether any of the small planets accessible to METIS are potentially habitable is clearly beyond the scope of this paper. To be sure, broader wavelength coverage is certainly required for an in-depth analysis of atmospheric features. However, it becomes more and more clear that life can exist over a broad temperature range and a current upper limit appears to be ~ 400 K (e.g. Seager 2013, and references therein). In addition, the basic concept of the 'habitable zone' around a star is undergoing major revisions, and of particular interest for the analyses presented here it seems that, under certain atmospheric conditions, the inner edge of the habitable zone around Solar-type stars extends much closer in and hence to higher equilibrium temperatures than originally thought (Zsom *et al.* 2013). To push the characterization aspect a bit further, possible next steps could be to replace the assumed black-body curves with more realistic atmospheric models with different compositions and resulting albedos. Not only will this help us to further refine the detection probabilities for different planet types, but we can also quantify to what degree the different spectroscopy modes of METIS and other future instruments could be used to further characterize the small planets that we can expect to find.

Conclusions

We explored two exoplanet science cases for the future 3–10 µm instrument METIS planned for the E-ELT. One of the key assumptions in our analyses is that METIS will be background limited at IWAs as small as $2\lambda_{cen}/D$, which is certainly technically challenging. We showed that already there is an interesting and sizable sample of RV-detected gas giant planets that METIS will be able to image directly within a reasonable amount of observing time. More than 20 objects covering a wide range of planetary masses and host star spectral types will be detectable in the L band, and half of those objects will also be seen in the M band given the detection limits we assume. With the continuation of RV searches for long-period planets and with the advent of the GAIA astrometry mission, many more, and perhaps better suited, targets will be added to the list in the future. Studying those objects in a grander sample with METIS will allow us for the first time to test and refine atmospheric models for planets

where the distance, and the object's mass, orbit and luminosity are empirically determined.

In addition to detecting cool gas giant planets, we showed that E-ELT/METIS could be the first instrument that might image a small and potentially rocky planet around one of the nearest stars. Based on the Kepler statistics METIS might detect ≈ 10 planets within 15 pc in at least one band (L, M or N). The L band offers the broadest discovery space for all planet–star combinations we analysed. Roughly five objects should be observable in both L and M bands, and for a couple of objects we might get a detection in N, L and/or M. Statistically speaking, most of these planets are expected to have equilibrium temperatures between 300 and 500 K, and at least a quarter of them will have a radius between 1 and $2 R_\oplus$. Hence, if those planets do exist around some of the nearest stars, METIS might reveal an object with potentially habitable conditions.

References

Amara, A. & Quanz, S.P. (2012). *Mon. Not. R. Astron. Soc.* **427**, 948.

Baraffe, I., Chabrier, G., Barman, T.S., Allard, F. & Hauschildt, P.H. (2003). *Astron. Astrophys.* **402**, 701.

Beuzit, J.-L. *et al.* (2006). *Messenger* **125**, 29.

Biller, B.A. *et al.* (2013). *Astrophys. J.* **777**, 160.

Birkby, J.L., de Kok, R.J., Brogi, M., de Mooij, E.J.W., Schwarz, H., Albrecht, S. & Snellen, I.A.G. (2013). *Mon. Not. R. Astron. Soc.* **436**, L35.

Boccaletti, A., Pantin, E., Lagrange, A.-M., Augereau, J.-C., Meheut, H. & Quanz, S.P. (2013). *Astron. Astrophys.* **560**, A20.

Boyajian, T.S. *et al.* (2012a). *Astrophys. J.* **746**, 101.

Boyajian, T.S. *et al.* (2012b). *Astrophys. J.* **757**, 112.

Boyajian, T.S. *et al.* (2013). *Astrophys. J.* **771**, 40.

Brandl, B.R. *et al.* (2012). In Society of Photo-Optical Instrumentation Engineers (SPIE) Conf. Ser., Vol. 8446.

Brogi, M., Snellen, I.A.G., de Kok, R.J., Albrecht, S., Birkby, J. & de Mooij, E.J.W. (2012). *Nature*, **486**, 502.

Burrows, A., Hubbard, W.B., Lunine, J.I. & Liebert, J. (2001). *Rev. Mod. Phys.* **73**, 719.

Carlotti, A. (2013). *Astron. Astrophys.* **551**, A10.

Carson, J. *et al.* (2013). *Astrophys. J.* **763**, L32.

Cassan, A. *et al.* (2012). *Nature* **481**, 167.

Chabrier, G., Baraffe, I., Allard, F. & Hauschildt, P. (2000). *Astrophys. J.* **542**, 464.

Chauvin, G., *et al.* (2010). *Astron. Astrophys.*, **509**, A52 + .

Crossfield, I.J.M. (2013). *Astron. Astrophys.* **551**, A99.

Cutri, R.M. *et al.* (2003). 2MASS All Sky Catalog of point sources. NASA/IPAC Infrared Science Archive.

Des Marais, D.J., Harwit, M.O., Jucks, K.W., Kasting, J.F., Lin, D.N.C., Lunine, J.I., Schneider, J., Seager, S., Traub, W.A. & Woolf, N.J. (2002). *Astrobiology* **2**, 153.

Dumusque, X. *et al.* (2012). *Nature* **491**, 207.

Fortney, J.J., Marley, M.S., Saumon, D. & Lodders, K. (2008). *Astrophys. J.* **683**, 1104.

Guyon, O. (2005). *Astrophys. J.* **629**, 592.

Hatzes, A.P. *et al.* (2000). *Astron. J.* **544**, L145.

Heinze, A.N., Hinz, P.M., Sivanandam, S., Kenworthy, M., Meyer, M. & Miller, D. (2010). *Astrophys. J.* **714**, 1551.

Henry, T.J. & McCarthy, D.W. Jr. (1993). *Astron. J.* **106**, 773.

Hinz, P.M., Kenyon, S., Meyer, M.R., Boss, A. & Angel, R. (2009). *astro 2010: The Astronomy and Astrophysics Decadal Survey*. **2010**, 126.

Hinz, P.M., Rodigas, T.J., Kenworthy, M.A., Sivanandam, S., Heinze, A.N., Mamajek, E.E. & Meyer, M.R. (2010). *Astrophys. J.* **716**, 417.

Howard, A.W. *et al.* (2012). *Astrophys. J. Suppl.* **201**, 15.

Hu, R., Ehlmann, B.L. & Seager, S. (2012). *Astrophys. J.* **752**, 7.

Janson, M., Bonavita, M., Klahr, H., Lafrenière, D., Jayawardhana, R. & Zinnecker, H. (2011). *Astrophys. J.* **736**, 89.

Janson, M. *et al.* (2013). *Astrophys. J.* **773**, 73.

Kalas, P., Graham, J.R., Chiang, E., Fitzgerald, M.P., Clampin, M., Kite, E. S., Stapelfeldt, K., Marois, C. & Krist, J. (2008). *Science* **322**, 1345.

Kenworthy, M.A., Quanz, S.P., Meyer, M.R., Kasper, M.E., Lenzen, R., Codona, J.L., Girard, J.H. & Hinz, P.M. (2010). In Society of Photo-Optical Instrumentation Engineers (SPIE) Conf. Ser., Vol. 7735.

Kuzuhara, M. *et al.* (2013). *Astrophys. J.* **774**, 11.

Lafrenière, D. *et al.* (2007). *Astrophys. J.* **670**, 1367.

Lagrange, A.-M. *et al.* (2010) *Science* **329**, 57.

Lagrange, A.-M., De Bondt, K., Meunier, N., Sterzik, M., Beust, H. & Galland, F. (2012). *Astron. Astrophys.* **542**, A18.

Lee, J.-M., Heng, K. & Irwin, P.G.J. (2013). *Astrophys. J.* **778**, 97.

Macintosh, B. *et al.* (2006) In Society of Photo-Optical Instrumentation Engineers (SPIE) Conf. Ser., Vol. 6272.

Marcy, G.W. *et al.* (2014). *Astrophys. J. Suppl.* **210**, 20.

Marley, M.S., Fortney, J.J., Hubickyj, O., Bodenheimer, P. & Lissauer, J.J. (2007). *Astrophys. J.* **655**, 541.

Marois, C., Lafrenière, D., Doyon, R., Macintosh, B. & Nadeau, D. (2006). *Astrophys. J.* **641**, 556.

Marois, C., Macintosh, B., Barman, T., Zuckerman, B., Song, I., Patience, J., Lafrenière, D. & Doyon, R. (2008). *Science* **322**, 1348.

Marois, C., Zuckerman, B., Konopacky, Q.M., Macintosh, B. & Barman, T. (2010). *Nature* **468**, 1080.

Mawet, D. *et al.* (2013). *Messenger* **152**, 8.

Mayor, M. & Queloz, D. (1995). *Nature* **378**, 355.

Mayor, M. *et al.* (2011). arXiv e- prints.

Meshkat, T. *et al.* (2013). *Astrophys. J.* **775**, L40.

Monet, D.G. *et al.* (2003). *Astron. J.* **125**, 984.

Nielsen, E.L. *et al.* (2013). *Astrophys. J.* **776**, 4.

Pepe, F., Lovis, C., Ségransan, D., Benz, W., Bouchy, F., Dumusque, X., Mayor, M., Queloz, D., Santos, N.C. & Udry, S. (2011). *Astron. Astrophys.* **534**, A58.

Perryman, M.A.C. *et al.* (1997). *Astron. Astrophys.* **323**, L49.

Petigura, E.A., Howard, A.W. & Marcy, G.W. (2013). *Proc. Natl. Acad. Sci. USA*, **110**, 19273.

Quanz, S.P., Amara, A., Meyer, M.R., Kenworthy, M.A., Kasper, M. & Girard, J.H. (2013). *Astrophys. J.* **766**, L1.

Rameau, J. *et al.* (2013a). *Astrophys. J.* **772**, L15.

Rameau, J., Chauvin, G., Lagrange, A.-M., Klahr, H., Bonnefoy, M., Mordasini, C., Bonavita, M., Desidera, S., Dumas, C. & Girard, J.H. (2013b). *Astron. Astrophys.* **553**, A60.

Schmid, H.M. *et al.* (2006). In *IAU Colloq. 200: Direct Imaging of Exoplanets: Science & Techniques*, ed. Aime, C. & Vakili, F. pp. 165–170.

Schneider, J., Dedieu, C., Le Sidaner, P., Savalle, R. & Zolotukhin, I. (2011). *Astron. Astrophys.* **532**, A79.

Seager, S. (2013). *Science* **340**, 577.

Seager, S. & Deming, D. (2010). *Annu. Rev. Astron. Astrophys.* **48**, 631.

Skemer, A.J. *et al.* (2012). *Astrophys. J.* **753**, 14.

Snellen, I.A.G., de Kok, R.J., de Mooij, E.J.W. & Albrecht, S. (2010). *Nature* **465**, 1049.

Spiegel, D.S. & Burrows, A. (2012). *Astrophys. J.* **745**, 174.

Sudarsky, D., Burrows, A. & Hubeny, I. (2003). *Astrophys. J.* **588**, 1121.

Tinney, C.G., Butler, R.P., Jones, H.R.A., Wittenmyer, R.A., O'Toole, S., Bailey, J. & Carter, B.D. (2011). *Astrophys. J.* **727**, 103.

Tuomi, M. *et al.* (2013). *Astron. Astrophys.* **551**, A79.

Vogt, S.S. *et al.* (2010). *Astrophys. J.* **708**, 1366.

Wahhaj, Z. *et al.* (2013). *Astrophys. J.* **773**, 179.

Zacharias, N., Finch, C.T., Girard, T.M., Henden, A., Bartlett, J.L., Monet, D.G. & Zacharias, M.I. (2012). *VizieR Online Data Catalog*, **1322**, 0.

Zsom, A., Seager, S., de Wit, J. & Stamenkovic, V. (2013). *Astrophys. J.* **778**, 109.